Monthly Notices of the ROYAL ASTRONOMICAL SOCIETY

MNRAS **536,** 2993–3006 (2025) https://doi.org/10.1093/mnras/stae2782
Advance Access publication 2024 December 19

Gargantuan chaotic gravitational three-body systems II. Dependence on angular momentum and astrophysical scale

T. C. N. Boekholt [1,2]★ and S. F. Portegies Zwart[3]★

[1]*Rudolf Peierls Centre for Theoretical Physics, Clarendon Laboratory, University of Oxford, Parks Road, Oxford, OX1 3PU, UK*
[2]*NASA Ames Research Center, Moffett Field, CA 94035, USA*
[3]*Leiden Observatory, Leiden University, PO Box 9513, NL-2300 RA, Leiden, The Netherlands*

Accepted 2024 December 13. Received 2024 December 6; in original form 2023 November 13

ABSTRACT

Recently, we estimated that about 5 per cent of unstable supermassive black hole triple systems are fundamentally unpredictable. These gargantuan chaotic systems are able to exponentially magnify Planck length perturbations to astronomical scales within their dynamical lifetime. These results were obtained in the zero angular momentum limit, which we naively expected to be the most chaotic. Here, we generalize to weakly and non-hierarchical triple systems with a range of non-zero angular momenta by systematically varying the initial virial ratio. We find the surprising result that increasing the angular momentum enhances their ability to amplify small perturbations, which we tracked up to 90 orders of magnitude using the arbitrary-precision N-body code BRUTUS. This result is partially explained by the fact that triples with higher angular momenta have longer lifetimes, allowing for a prolonged exponential growth. However, we also find that for a fixed lifetime, triples with higher angular momenta can amplify perturbations to larger values, indicating that the Lyapunov exponent is also a function of angular momentum. These empirical results provide targets for three-body theories which invoke chaos drivers such as resonance overlap and punctuated chaos. Comparing the zero angular momentum case to our new ensembles with higher angular momenta, we conclude that the percentage of unpredictable supermassive black hole triples increases up to about 30 per cent. A further increase up to about 50 per cent is reached when considering triples on smaller astrophysical scales. Fundamental unpredictability is thus a generic feature of chaotic, self-gravitating triple populations.

Key words: methods: numerical – stars: kinematics and dynamics.

1 INTRODUCTION

The gravitational three-body problem (Newton 1687) is ubiquitous in the Universe. Examples range from the Sun–Earth–Moon system (e.g. Touma & Wisdom 1998), to Trans-Neptunian triplets (e.g. Correia 2018), Jacobi captures (e.g. Boekholt, Rowan & Kocsis 2023b), hierarchical triple stars (e.g. Toonen, Boekholt & Portegies Zwart 2022), stellar-mass black holes (e.g. Portegies Zwart & McMillan 2000; Samsing, MacLeod & Ramirez-Ruiz 2014), supermassive black holes (e.g. Kollatschny et al. 2020; Boekholt, Moerman & Portegies Zwart 2021), and even whole galaxies (Väisänen et al. 2008).

Chaos in the gravitational three-body problem was first demonstrated by Henri Poincaré (Poincaré 1891, 1892). It manifests itself through the exponential sensitivity to small perturbations (Miller 1964; Dejonghe & Hut 1986; Goodman, Heggie & Hut 1993). If the finite-mass third body is infinitely far away, the motions of the other two bodies can be obtained analytically by solving the Kepler-problem (Kepler 1609). If the third body is systematically brought closer to the other two bodies, its gravitational influence increases, and through sequences of close encounters (e.g. Portegies Zwart, Boekholt & Heggie 2023; Boekholt, Portegies Zwart & Heggie 2023a) and orbital resonances (e.g. Mardling 2008), the gravitational interaction becomes increasingly chaotic. Here, we define chaotic response as the exponential growth of any small perturbation in the motion of the three bodies, and regular response when the growth is weaker than exponential.

The motion in non-hierarchical three-body systems is characterized by a series of transitions between regular and chaotic motion. This behaviour manifests itself in sequences of short democratic resonances, during which all pairwise distances are of the same order, alternated by extended phases of hierarchical evolution, during which one of the bodies is on an excursion away from the remaining pair (McMillan & Hut 1996). This latter phase can be represented by Lévy flights (Stone & Leigh 2019; Manwadkar, Trani & Leigh 2020) in phase space. However, not all variations and transitions in the exponential growth rate can be explained this way, indicating the presence of other mechanisms also affecting the rate of divergence (Portegies Zwart & Boekholt 2018; Portegies Zwart et al. 2023).

To mediate the discussion we will quantify chaotic motion by a measure of the local Lyapunov time-scale T_λ (Portegies Zwart & Boekholt 2018). This measure is the reciproke of the local, finite-time, maximum Lyapunov exponent of a system. The value of this chaotic quantifier is local (in time), and although its value can

★ E-mail: tjarda.boekholt@nasa.gov (TB); spz@strw.leidenuniv.nl (SPZ)

vary considerably from one moment to the next, the global trend is surprisingly stable. This leads to well-defined averaged Lyapunov exponents, which are an inherent property of chaotic N-body systems (Boekholt, Portegies Zwart & Valtonen 2020; Portegies Zwart et al. 2023). The relation between the Lyapunov exponent of a system and the detailed motions of the three bodies is still an open problem. Lines of investigation include orbital resonances and resonance overlap (e.g. Mardling 2008), or sequences of strong two-body encounters and deflections (Goodman et al. 1993; Boekholt et al. 2016), i.e. punctuated chaos (Portegies Zwart et al. 2023).

Irrespective of the mechanism that drives the exponential divergence between two neighbouring trajectories in phase space, exponential sensitivity can be measured through performing accurate and precise N-body simulations (Boekholt et al. 2020). Here, the accuracy reflects a measure to which energy is conserved, and precision can be perceived as the number of decimal places used to express the result (Portegies Zwart & Boekholt 2018). Boekholt et al. (2020; hereafter Paper 1) studied triples systematically drawn from the Agekyan–Anosova map (Agekyan & Anosova 1967, 1968), and measured a power-law distribution of amplification factors, e.g. the amplification factor of a small initial perturbation over the lifetime of the triple. The implication is the presence of a power-law tail of triple systems, which produce extremely large amplification factors, i.e. gargantuan chaotic triple systems. We found a finite fraction of systems that would remain irreversible, even if the calculations would be conducted with a precision below the Planck length. We therefore argued that these gargantuan chaotic systems would be fundamentally irreversible and unpredictable. Despite our lack of understanding on the deterministic behaviour of quantum gravity at sub-Planck length scales and considering Heisenberg's principle of uncertainty, we argue that this irreversible fraction may be fundamental to the arrow of time (Portegies Zwart & Boekholt 2023). Recent binary-single scattering experiments by Trani et al. (2024) also revealed a sensitivity to the Planck length scale due to the presence of an underlying multi-fractal structure, which was resolved using the arbitrary-precision N-body code BRUTUS (Boekholt & Portegies Zwart 2015).

In Paper 1, we focused on the amplification factor for zero-angular momentum orbits, naively assuming that those would be more chaotic than configurations with non-zero angular momentum. Our naivety in the zero-angular momentum problem stems from the fact that for two-body problems, smaller angular momentum implies more radial orbits. As a consequence, and extrapolating to three-body systems, this naturally leads to close encounters. On the other hand, bodies in configurations with finite angular momentum would remain on average at larger distance from each other, leading to fewer and weaker interactions. Based on such an intuition it might be argued that zero-angular momentum systems would be maximally chaotic. As it turns out now, as we explain in this paper, this only holds statistically for the shortest lived triple systems (up to about 20 crossing times). We find the surprising result that the opposite is true for longer lived systems (which are also the majority); more angular momentum in non-hierarchical or weakly hierarchical three-body initial conditions leads to longer lifetimes, shorter Lyapunov time-scales, larger magnification factors, and therefore to more chaos. Generally, when increasing the initial amount of angular momentum, the fraction of irreversible solutions increases. However, in the regime of high angular momenta, where triples tend to be hierarchical with much longer decay times, the fraction of irreversible solutions is expected to decrease again, and therefore we hypothesize that there should be a peak in the irreversible fraction at a certain characteristic angular momentum.

This second paper on gargantuan chaotic triples extends the results of Paper 1 to triples with non-zero angular momenta, but still in the regime where they are non-hierarchical or weakly hierarchical. We demonstrate that the fraction of unpredictable triples can reach larger values than found in Paper I. We will also scale the results to triples of arbitrary physical scale finding that the fraction of unpredictable triples is further enhanced for more compact triples, such as triple asteroids (see Section 4.2). Complementary to the intrinsic quantum perturbations, we will also briefly discuss tidal perturbations from the presence of other bodies in the Universe. In most cases these tend to dominate over intrinsic Planck length uncertainties, which enhances the unpredictability of N-body systems even further (see Section 4.3).

2 METHODS

2.1 Initial conditions

We adopt the equal mass Plummer distribution (Plummer 1911) for drawing random initial positions and velocities for the three bodies. The initial velocities will then be adjusted in order to vary the total angular momentum. This procedure will generally result in a non-hierarchical, unstable triple system. However, if the total angular momentum is larger than zero, a small fraction of random realisations can also have a weak hierarchy, i.e. a ratio of the outer orbit's pericenter divided by the inner orbit's semimajor axis in the range of 2–4, which puts it on the edge of (in)stability. In principle other initial conditions than the Plummer model could have been used, but the Plummer model is a well-known toy model for stellar systems, and allows for a natural extension from 2D (as in Paper I) to 3D (current study), as well as from $N = 3$ (current study) to larger N stellar systems (e.g. Portegies Zwart et al. 2022). Three-body Plummer models were also used by e.g. Portegies Zwart & Boekholt (2014) and Boekholt & Portegies Zwart (2015). Furthermore, we will show that for the case of zero angular momentum triples, we get consistent results with those of Paper I, which adopted the Agekyan–Anosova map. The statistical outcome of N-body simulations of chaotic systems is primarily determined by the global conserved quantities, i.e. energy and angular momentum (e.g. Portegies Zwart & Boekholt 2014).

The Plummer model was originally used for star clusters with a large value of N. In virial equilibrium the total kinetic energy, T, and potential energy, V, are related by $2T + V = 0$. Since the total energy is $E = T + V$, we can combine the two relations and write $E = \frac{1}{2}V$. This can be written in terms of the total mass, M, and virial radius, $R_{\rm V}$, of the cluster defined by

$$E = -\frac{1}{4}\frac{GM^2}{R_{\rm V}}, \tag{1}$$

with G the gravitational constant. The virial radius is used as a characteristic size of the Plummer sphere. Similarly, a characteristic time-scale is defined by $T = 2R_{\rm V}/\sigma$, with σ the mass-weighted velocity dispersion. This time-scale is commonly referred to as the dynamical time or crossing time of the cluster. Although originally defined for large-N star clusters, the Plummer model can be extrapolated downwards to the case of $N = 3$, thereby providing a method for the random generation of triples with mostly non-hierarchical configurations, a certain total mass, M, characteristic size, R_V, and a pre-defined crossing time. This is especially useful for non-hierarchical, chaotic systems in which there are no well-defined or long-lived Keplerian orbits.

For numerical implementation purposes it is useful to set $G = 1$. For rescaling purposes, one usually works with dimensionless units. The following scaling factors are introduced: $f_{\rm M} = M$, $f_r = R_{\rm V}$, $f_v = \sqrt{GM/R_{\rm V}}$, and $f_{\rm t} = f_r/f_v$, for the mass, positions, velocities and time, respectively. Given the initial condition in physical units, one makes them dimensionless by dividing by these scaling factors. After the simulations are finished, physical units are retrieved from the dimensionless units by multiplying the results by the scaling factors. The set of scaling factors defined above are widely used in the N-body community and originally called N-body units (e.g. Heggie & Mathieu 1986). They rescale the gravitational constant, dimensionless total mass and virial radius to unity. Since 2014, these set of dimensionless units are also known as Hénon units. The results in this paper will be given in Hénon units, but they are easily converted to physical units by defining the scaling factors as given above.

So far, the angular momentum, L, of the triple has not explicitly appeared yet. The method given above generates virialised triples with a well-defined mass and energy, while also fulfilling the virial relation $2T + V = 0$, but L varies among the different realisations. The average value for initially virialised triples is $\langle L_{\rm virial}\rangle = 0.19$ in Hénon units.

In order to generate ensembles of triples with a lower average angular momentum, we adjust the initial virial ratio, Q, which is defined as the ratio between total kinetic energy, T, and absolute value of the potential energy, V:

$$Q = \frac{T}{|V|}. \tag{2}$$

A triple with zero initial velocities has a virial ratio of $Q = 0$ and angular momentum $L = 0$. We can therefore create ensembles of triples with different angular momenta by rescaling the initial velocities. By systematically increasing the initial velocities, we increase both Q and L. The maximum angular momentum in our experiment corresponds to the case of the initially virialised triples. We leave the domain of triples with even higher values of L, which also tend to be mostly hierarchical triples, to a separate study.

The procedure for generating initial conditions starts by generating a random realisation of a virialised triple system drawn from a Plummer distribution. For the virial case we have the relation $2T + V = 0$, and therefore $Q = \frac{1}{2}$. To change the virial ratio we rescale the velocities, and therefore T, by a factor $C_{\rm V}$:

$$\frac{Q}{Q_{\rm V}} = \frac{T}{T_{\rm V}} = \left(\frac{\sigma}{\sigma_{\rm V}}\right)^2 \equiv C_v^2, \tag{3}$$

with σ the mass-weighted velocity dispersion, and the subscript V refers to virial. Since $Q_v = \frac{1}{2}$, we can write

$$C_v = \sqrt{2Q}. \tag{4}$$

This scaling of the velocities changes the total energy of the triple to a value

$$E_1 = \frac{1}{2}M\left(C_v\sigma_{\rm V}\right)^2 - \frac{1}{2}\frac{GM^2}{R_{\rm V}} = \frac{1}{4}C_v^2 - \frac{1}{2} = \frac{Q}{2} - \frac{1}{2}, \tag{5}$$

whereas its initial virialised value was set to $E_0 = -\frac{1}{4}$. In order to normalize the energy, we calculate the scaling factor of the total energy

$$C_{\rm E} \equiv \frac{E_0}{E_1} = \frac{1}{2 - C_{\rm V}^2} = \frac{1}{2-2Q} \tag{6}$$

and rescale the positions and velocities by factors respectively given by

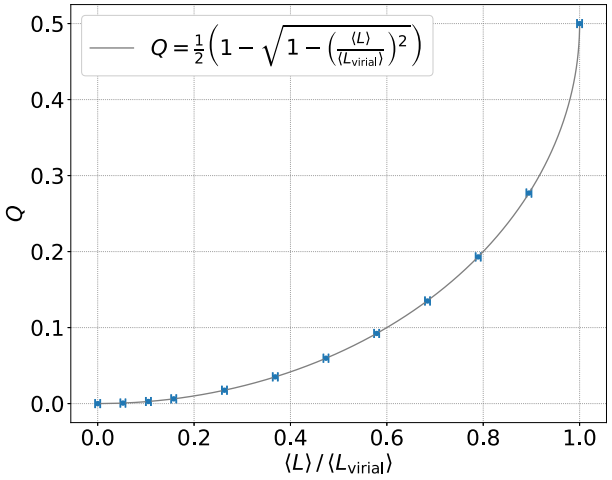

Figure 1. Relation between virial ratio, Q, and angular momentum, L. Our ensembles of triple systems vary L systematically and are confined to be within the horizontal 'error bars'.

$$D_r \equiv \frac{1}{C_{\rm E}} = 2 - C_{\rm V}^2 = 2 - 2Q, \tag{7}$$

$$D_v \equiv \sqrt{C_{\rm E}} = \frac{1}{\sqrt{2 - C_{\rm V}^2}} = \frac{1}{\sqrt{2-2Q}}, \tag{8}$$

which rescales the total energy back to a value E_0, while preserving the virial ratio Q. The total angular momentum scales as

$$\frac{L}{L_{\rm V}} = D_r C_v D_v = \frac{\sqrt{2Q}\,(2-2Q)}{\sqrt{2-2Q}} = 2\sqrt{Q\,(1-Q)}, \tag{9}$$

where D_r is the net scaling of the positions, and $C_v D_v$ is the net scaling of the velocities. From this expression we confirm that for $Q = 0$ we obtain $L = 0$, while for $Q = \frac{1}{2}$ we retrieve $L = L_{\rm V}$. Hence, with this relation between L and Q, we can generate ensembles of non/weakly-hierarchical triples with a varying amount of angular momentum. However, the drawing of random realisations of triple systems for a given value of Q still results in a spread of values for L. The average value of L however does scale one-to-one with Q, and we therefore use

$$\frac{\langle L\rangle}{\langle L_{\rm virial}\rangle} = 2\sqrt{Q\,(1-Q)}, \tag{10}$$

or after inverting the equation we obtain

$$Q = \frac{1}{2}\left(1 - \sqrt{1 - \left(\frac{\langle L\rangle}{\langle L_{\rm virial}\rangle}\right)^2}\right). \tag{11}$$

Henceforth, we might omit the angular brackets (L instead of $\langle L\rangle$) for simplicity, i.e. L refers to the average value of the ensemble unless stated otherwise. In Fig. 1, we plot the relation between Q and L. We define 12 ensembles of triple systems for which the average angular momentum is systematically varied. For each ensemble, we calculate the corresponding value for Q. Then we generate 2048 random, virialised triple realisations, which we subsequently rescale according to the procedure described above. Since we are interested in measuring trends with L, we do not want the range in L within an ensemble to be too broad. Therefore, we only accept a random realisation of a triple if its angular momentum is within the range given by $L \pm \delta L$ with $\delta L = 0.001$. For the virialised case, this margin corresponds to $\delta L/L_{\rm virial} = 0.0053$. The corresponding values of L and Q are given in Table 1, and the ensembles are also presented

Table 1. Table of initial conditions and statistical outcomes. The relation between virial ratio, Q, and angular momentum, L, is visualized in Fig. 1. The parameters ν and η correspond to the linear fits in Fig. 2. The parameters α and β correspond to the linear fits in Fig. 5. The parameter p refers to the percentage of fundamentally unpredictable triples in our massive black hole application (see Section 4).

$\langle L\rangle/\langle L_{\rm virial}\rangle$	$\langle L\rangle$	Q	ν	$\delta\nu$	η	$\delta\eta$	α	$\delta\alpha$	β	$\delta\beta$	p (per cent)	δp (per cent)
1.00	0.19	0.5	0.0115	0.0003	0.060	0.003	0.83	0.01	0.12	0.02	29.8	0.4
0.895	0.17	0.277	0.0131	0.0004	0.074	0.003	0.88	0.01	0.06	0.02	25.4	0.5
0.790	0.15	0.193	0.0147	0.0002	0.079	0.002	0.86	0.02	0.08	0.03	21.5	0.2
0.684	0.13	0.135	0.0170	0.0001	0.089	0.001	0.82	0.02	0.15	0.02	16.6	0.1
0.579	0.11	0.0923	0.0206	0.0005	0.106	0.005	0.80	0.02	0.18	0.03	11.4	0.3
0.474	0.09	0.0597	0.0237	0.0003	0.125	0.002	0.76	0.01	0.23	0.02	8.2	0.1
0.368	0.07	0.0352	0.0270	0.0005	0.147	0.004	0.79	0.02	0.19	0.03	5.9	0.2
0.263	0.05	0.0176	0.030	0.001	0.163	0.009	0.71	0.01	0.29	0.02	4.2	0.2
0.158	0.03	0.00627	0.0322	0.0006	0.172	0.005	0.68	0.01	0.31	0.02	3.4	0.1
0.105	0.02	0.00278	0.033	0.001	0.18	0.01	0.75	0.02	0.17	0.02	3.1	0.2
0.0524	0.01	0.000693	0.0291	0.0007	0.154	0.005	0.66	0.02	0.34	0.03	4.7	0.2
0.0	0.0	0.0	0.0282	0.0006	0.151	0.005	0.75	0.01	0.19	0.02	5.2	0.2

in Fig. 1 as the horizontal 'errorbars'. It is clear that the various ensembles do not overlap, which allows us to measure statistical trends as a function of angular momentum.

2.2 Experimental setup

Adopting the same strategy as Portegies Zwart & Boekholt (2018) and Boekholt et al. (2020), we use the code BRUTUS (Boekholt & Portegies Zwart 2015) to perform a reversibility test. Each initial condition is integrated forwards in time until dissolution of the triple configuration. We define this to be the case if one of the bodies (1) is at a distance beyond 10 Hénon length units from the centre of mass of the triple, (2) is moving away from the centre of mass, and (3) has a positive energy, meaning it has become unbound from the remaining binary system. Since a small fraction of triples is very long lived, we also set a maximum simulation time of 10^4 Hénon time units, or about 3536 crossing times ($T_{\rm c}$). We define the duration of the forward integration from the initial condition to the stopping conditions as the lifetime, T, of the triple. At that moment, we flip the sign of each velocity coordinate of each particle, and integrate forwards until a final simulation time of $t = 2T$. Note that effectively, the system is evolving back to the future initial condition. We can compare the initial (forward) and final (backward) configurations by measuring their phase space distance (note that the velocities of the backward integration have to be flipped again so that they have the same sign as the forward integration), given by

$$\Delta^2 = \sum_{i=1}^{N}\sum_{k=1}^{6}\left(x_{i,k,f} - x_{i,k,b}\right)^2, \tag{12}$$

where the first sum is over all bodies ($N = 3$), the second sum over all phase space coordinates (positions and velocities), and where the subscript f and b refer to the forward and backward integration, respectively. Or in words, the phase space distance, Δ, gives the Euclidean distance between the two solutions in $6N$-dimensional phase space. For a perfectly time-reversible integrator with reversible numerical errors, the phase space distance between the forward and backward solutions would remain zero. In this case, a reversibility test does not hold any information about the accuracy of the solution or the exponential sensitivity of the trajectory. However, in the presence of irreversible numerical errors, these errors will serve as a perturbation to the system, which seeds the exponential divergence between the forward and backward integrations, i.e. the phase space distance between the two solutions will grow exponentially. A reversibility test is then declared successful if the phase space distance between the initial and final states is below some small threshold, for which we adopt

$$\log_{10}\,\Delta \leq -3. \tag{13}$$

This criterion ensures we remain in the linear perturbation regime, as Δ remains a factor 10^3 smaller than the characteristic size and speed of the triple system. Remaining in the linear regime is critical as numerical errors will not have the opportunity to affect the solution on a macroscopic scale, such that the solution diverges to a quasi-random trajectory. Hence, this allows us to make accurate measurements of e.g. the lifetime of the triple and the maximum Lyapunov exponent, still belonging to that specific initial configuration. This approach is an application of the method of convergence used in conjunction with BRUTUS as described in detail by Boekholt & Portegies Zwart (2015), Portegies Zwart & Boekholt (2018), and Boekholt et al. (2020). In short, given a specific initial condition of an unstable triple system, there is a unique mathematical solution for the trajectories in time, which we deem the 'true' or 'correct' solution. Numerical errors perturb the trajectories away from the true solution, and if the perturbations reach the magnitude of the size of the triple itself, then the perturbations have become non-linear, and the numerical solution has become macroscopically different from the true solution. Using the BRUTUS code, we can prevent this from occurring by systematically controlling and reducing the magnitude of the numerical errors. Since N-body simulations define a limited simulation time, we find that there is a corresponding limited (maximum) magnitude for the errors, such that numerically diverging trajectories remain in the linear regime during the simulation. From that point onward, if we would continue to reduce the magnitude of the errors, we find that we are only increasing the number of converged decimal places, without affecting the macroscopic configuration anymore. Generating such numerically 'converged' solutions allows us to study chaotic N-body problems with solutions arbitrarily close to the true solution.

In our first attempt to obtain a reversible solution for each triple, we set the Bulirsch–Stoer tolerance parameter to $\epsilon = 10^{-6}$, and we express the word-length (length of the mantissa in units of bits) as

$$L_w = -4\log_{10}\,\epsilon + 32, \tag{14}$$

which for $\epsilon = 10^{-6}$ corresponds to 56 bits, and more bits are added as ϵ decreases (Boekholt & Portegies Zwart 2015). If the reversibility test fails for a subset of triples, then we redo the test with a smaller value of ϵ and the corresponding value of L_w. This way, we can measure the fraction of irreversible solutions as a function

of numerical accuracy and precision. We halted the iteration at $\epsilon = 10^{-90}$, but we will show that even then a fraction of triples still remained irreversible. Besides the fraction of irreversible solutions, we also measure the two main observables for each triple, which are the lifetime T, and the amplification factor defined as

$$A = \frac{\Delta_f}{\Delta_i}. \tag{15}$$

Here, Δ_i is the phase space distance between the forward and backward solution after a single integration step (i.e. the states just before and after $t = T$ are compared), and Δ_f is the phase space distance between the initial and final states. In other words, A gives the total amplification factor of the initial perturbation over the lifetime of the triple. The finite-time Lyapunov exponent is then estimated as

$$\lambda = \frac{\log A}{T}, \tag{16}$$

while the finite-time Lyapunov time-scale is the inverse, i.e. $T_\lambda = \lambda^{-1}$.

The underlying question in our experiment is: given a specific initial configuration, what is the maximum value of ϵ such that the phase space separation between the forward and backward integration remains in the linear regime throughout? Chaos prevents us from knowing this a priori; it depends on the lifetime of the interaction and the rate of exponential divergence, which, as we will show, varies among different three-body configurations. Our approach is then to perform multiple simulations of the same initial condition, but with smaller values of ϵ until convergence is achieved, i.e. the phase space separation between the forward and backward integration remains in the linear regime. Since our approach depends on the ability to remain in the linear regime, we require studying an ensemble of different initial triples. The alternative of creating an ensemble from a single triple with different initial small perturbations will lead to solutions which are the same in the linear regime, but which diverge only in the non-linear regime, at which point our approach for measuring the exponential growth rate becomes invalid, i.e. the exponential growth rate is truncated by the size of the triple.

3 RESULTS

We first present the outcome of the reversibility experiment in Section 3.1. There, we find that ensembles of triples with a higher angular momentum produce a larger fraction of irreversible solutions (see Figs 2 and 3). Similar to Paper 1 we find that this is correlated with having larger amplification factors (see Fig. 4). In Section 3.2, we explore the correlation between the two main observables: amplification factors and lifetimes (see Figs 5–7). We will show that higher angular momentum triples can achieve larger amplification factors both due to longer lifetimes as well as larger Lyapunov exponents (see Figs 8 and 9). In Section 4, we discuss how the results scale with astrophysical size, and we will also apply our results to tidal perturbations from other bodies in the Universe, which complement intrinsic quantum uncertainties.

3.1 Reversibility test

In Fig. 2, we plot the fraction of irreversible integrations, $f_{\rm irr}$, as a function of numerical accuracy, i.e. Bulirsch–Stoer tolerance, ϵ. For each value of the total angular momentum, we find that the data follows a power law. At low accuracy (large ϵ), $f_{\rm irr}$ is of order unity, and with increasing accuracy (smaller ϵ), this fraction decreases

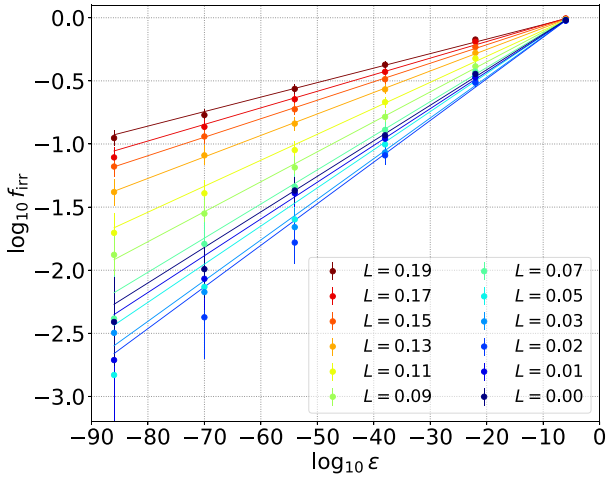

Figure 2. Fraction of irreversible simulations, $f_{\rm irr}$, as a function of integration accuracy, which is represented by the Bulirsch–Stoer tolerance, ϵ. The data points and errorbars are obtained from the data, while the curves are linear fits whose parameters are given in Table 1, with ν the slope and η the offset. Higher angular momentum triples have a larger fraction of irreversible solutions. Interestingly, we observe that the lowest irreversible fraction is produced by $L = 0.02$ rather than $L = 0$. This turns out to be correlated with statistically shorter lifetimes (see Fig. 4).

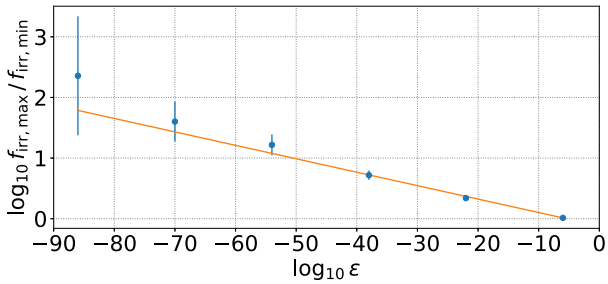

Figure 3. We plot the ratio between the largest and smallest irreversible fraction from Fig. 2, i.e. between those of $L = 0.19$ and $L = 0.02$. We fit a linear relation resulting in a slope -0.022 ± 0.001 and offset -0.120 ± 0.008.

according to a power law. The power-law index however, depends on angular momentum. We perform linear fits to the data

$$\log_{10} f_{\rm irr} = \nu \log_{10} \epsilon + \eta, \tag{17}$$

where the fit parameters, ν and η, can be found in Table 1. For the case of $L = 0$, we measure a power-law index of $\nu = 0.0282 \pm 0.0006$, which is consistent with the measurement of 0.029 ± 0.001 for the Agekyan–Anosova map of initial conditions from Paper 1. As we increase the total angular momentum, we find that the power-law index first increases to a maximum value of $\nu = 0.033 \pm 0.001$ for $L = 0.02$, and then decreases monotonically until a value of $\nu = 0.0115 \pm 0.0003$ for the initially virialized ensemble. Hence, the easiest triples to reverse have $L = 0.02$, while the hardest triples to reverse are the virial ones with $L = 0.19$. In Fig. 3 we plot the ratio between the largest and smallest fractions from Fig. 2, which are those for $L = 0.02$ and $L = 0.19$. It is striking that for $\epsilon = 10^{-90}$, the range in $f_{\rm irr}$ among the ensembles is two orders of magnitude, with approximately 10 per cent of triples being irreversible still for $L = 0.19$.

In Paper 1, we demonstrated that the fraction of irreversible solutions is determined by the distribution of amplification factors.

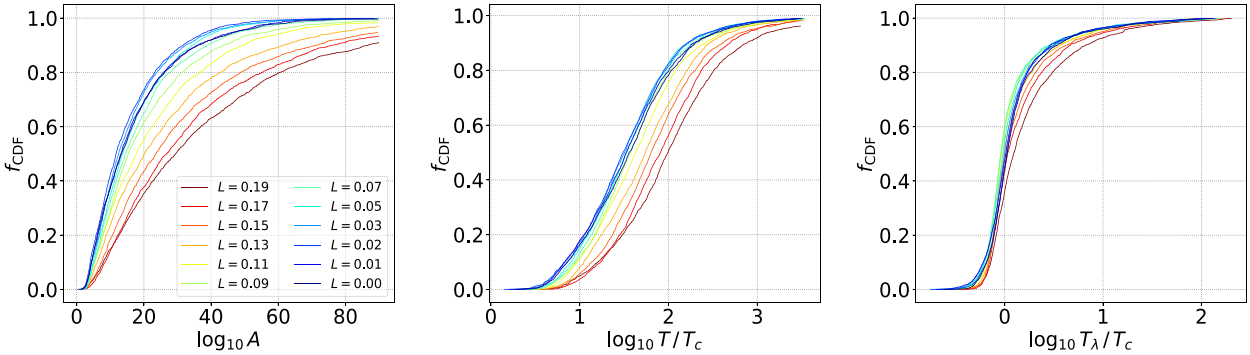

Figure 4. Cumulative distribution functions of the amplification factor (left), lifetime (middle), and Lyapunov time-scale (right). Triples with larger L have statistically larger amplification factors and lifetimes. For the smallest L values, we observe that $L = 0.02$ statistically produces the smallest amplifications rather than $L = 0$. Two-sample Kolmogorov–Smirnoff tests between the distributions of $L = 0$ and $L = 0.19$ give p-values smaller than 10^{-22} for each of the three distributions, indicating that all three quantities have a L-dependence, including the Lyapunov time-scale. Comparing $L = 0$ and $L = 0.02$ we obtain p-values of 0.00018, 0.0044 and 0.71 (from left to right panel respectively). Hence, the observation that $L = 0.02$ produces smaller values of A than $L = 0$ is most likely explained by statistically shorter lifetimes, and not by different Lyapunov time-scales. We also confirm that the median Lyapunov time-scale is of order the crossing time.

In Fig. 4 (left panel), we plot the cumulative distribution function of $\log_{10} A$ for the various ensembles of triples. We confirm that the distributions are angular momentum dependent, such that higher angular momentum triples produce larger amplification factors. We observe that for $L = 0.19$, about 10 per cent of triples amplify the initial perturbation by more than a factor of 10^{90}. Here, we also observe that the ensemble of triples with $L = 0.02$ produces the smallest amplifications in a statistical sense. Our observations of the L-dependence of $f_{\rm irr}$ in Fig. 2 are thus reflected in the distributions of A in Fig. 4 (left panel). The relation between reversibility and amplification factor was previously discussed by Portegies Zwart & Boekholt (2018) and Boekholt et al. (2020).

The amplification is determined by the lifetime of the interaction during which perturbations can be amplified, and the instantaneous Lyapunov exponent, which gives the rate of amplification in time. The L-dependence of the amplification factor can thus be a consequence of an L-dependence of the lifetime and/or Lyapunov time. In Fig. 4, we plot their respective cumulative distribution functions. We adopt the two-sample Kolmogorov–Smirnoff (KS) test in order to test whether the various empirical distributions could have been drawn from the same underlying distribution, or whether they are significantly different. We first compare $L = 0$ and $L = 0.19$ in each of the three panels of Fig. 4. The KS test produces p-values smaller than 10^{-22} for each of the three distributions, confirming that all three quantities have a statistically significant L-dependence. This includes the Lyapunov time-scale. Whereas the statistical longer lifetimes for $L = 0.19$ (middle panel of Fig. 4) would contribute towards producing larger amplification factors (left panel), the statistical distribution of Lyapunov times is also shifted towards (somewhat) larger values (right panel), indicating slower growth rates. Nevertheless, the net result is an increase of the amplification factor. When multiplying the lifetimes by a constant Lyapunov exponent, we find that this does not reproduce the distribution of amplification factors. The L-dependence of the amplification factor is thus determined by the L-dependence of both the lifetime and the Lyapunov time. We will continue this analysis in the next subsection.

First, we seek a better understanding of why $L = 0.02$ rather than $L = 0$ seems to be the easiest ensemble to reverse. We perform KS tests comparing $L = 0$ and $L = 0.02$ obtaining p-values of 0.00018, 0.0044, and 0.71 for A, T, and T_λ, respectively. At a confidence level of 95 per cent, we conclude that the distributions of A and T are not drawn from the same underlying distribution, but that T_λ is. Hence, this suggests that $L = 0.02$ triples are easier to reverse because they have systematically shorter lifetimes. We leave a physical explanation for this observation in terms of detailed orbital dynamics for follow up studies, although we present some first attempts in Section 3.3. Finally, we observe that the median of the Lyapunov time-scale is of order the crossing time (right panel of Fig. 4), which is consistent with the theory of punctuated chaos (Portegies Zwart et al. 2023).

3.2 Correlating amplification factors and lifetimes

Our next step is to better understand why high angular momentum triples produce larger amplification factors. One contributing factor is that on average high angular momentum triples have longer lifetimes than low angular momentum triples (e.g. Orlov, Rubinov & Shevchenko 2010; Boekholt & Portegies Zwart 2015). However, we find that simply multiplying the lifetimes of the triples by a constant Lyapunov exponent does not reproduce the measured distribution of amplification factors. Rather than writing

$$\log A\,(L) = \lambda T\,(L)\,, \tag{18}$$

with λ a constant Lyapunov exponent, we require the more general case given by

$$\log A\,(L) = \lambda\,(T, L)\,T\,(L)\,, \tag{19}$$

where the finite-time Lyapunov exponent itself is a function of lifetime and angular momentum (e.g. Mikkola & Tanikawa 2007; Urminsky & Heggie 2009).

The discussion above motivates the inspection of the correlation between the two main observables in our experiments, namely the amplification factor, A, and the lifetime, T. In Fig. 5, we present scatter plots of these two quantities for each of our angular momentum ensembles. After experimenting with various combinations of linear and logarithmic axes, we find that a clean linear relation is obtained in the space of $\log\log A$ versus $\log T$. The first observation we make is that for each given T, there is a (sharp-edged) maximum value of A. This diagonal upper ridge continues up to about $100\,T_{\rm c}$, after which A flattens. By this time, A has reached a value of 10^{90}, which is the limit in our experiment. If we had continued to decrease the Bulirsch–Stoer tolerance beyond 10^{-90}, we expect the diagonal trend to continue. Hence, if we only consider the resolved portion

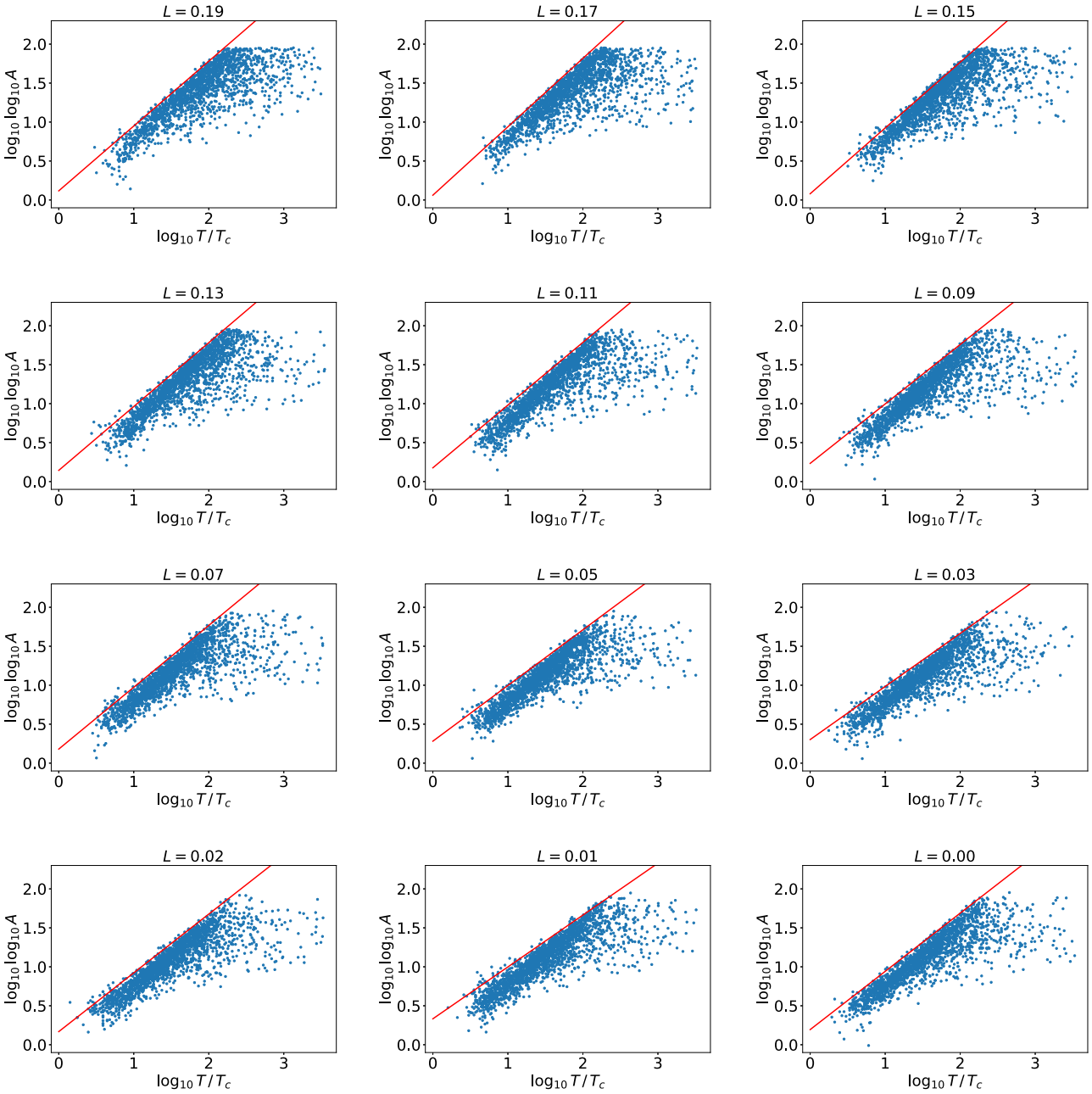

Figure 5. Scatter plots of the two main observables: amplification factor, A, and lifetime, T (normalized by crossing time, T_c). We estimate the slope of the upper edge of the data using linear fits (solid lines). The fit parameters are given in Table 1 with α the slope and β the offset. The angular momentum dependence of the slope is visualized in Fig. 6.

of the scatter plot ($T \leq 100\,T_c$), we observe a sharp upper ridge in the data, which is indicative of a maximum Lyapunov exponent, i.e. a maximum rate of divergence. The second observation is the gradual scatter of data points towards very long lifetimes. The maximum lifetime in our experiment was set to 10^4 Hénon time units ($\sim$3536 T_c). There is a large range of lifetimes, which still end up with the same amplification factor. This observation can be interpreted by stating that the evolution of long-lived triples is driven by prolonged excursions of a single body during which it is only weakly interacting with the binary system. The exponential sensitivity during these phases is greatly reduced (see also Fig. 9).

Coming back to the first observation, we fit the upper edge of the resolved data with a linear model,

$$\log_{10}\log_{10} A = \alpha \log_{10} \frac{T}{T_c} + \beta, \tag{20}$$

where the fitting parameters, α and β, are given in Table 1. Here, we made bins along the horizontal axis, and used a bootstrap resampling method to estimate error margins to the fitting parameters. In Fig. 6, we plot the slopes of the linear fits, α, as a function of angular momentum: high angular momentum triples have a steeper slope, i.e. α increases from $\sim$0.70 to $\sim$0.86. The implication is best observed in Fig. 7. There, we find that up to about 20 T_c the largest amplification

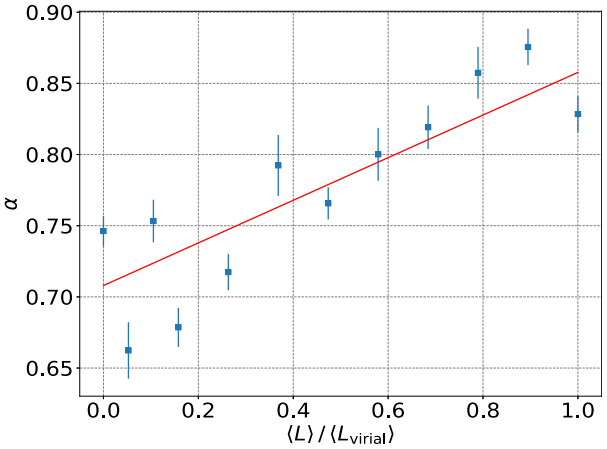

Figure 6. Angular momentum dependence of the slope of the linear fits in Fig. 5. A linear fit to the data points (solid line) indicates an upward trend. This implies that triples with more angular momentum are able to reach larger amplification factors. This is further visualized in Fig. 7.

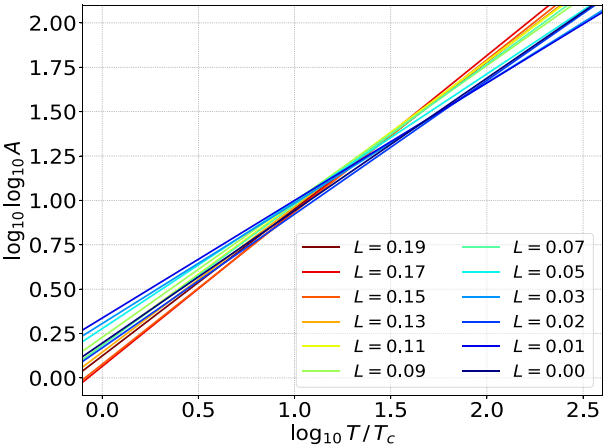

Figure 7. We collect the linear fits from Fig. 5 for a direct comparison. Initially, up to about 20 crossing times, larger amplification factors are reached by the low angular momentum triples. At longer lifetimes however, the high angular momentum triples take over.

factors are reached by the lower angular momentum triples. At longer times however, the higher angular momentum triples become dominant, e.g. larger values of A by $\sim$14 orders of magnitude for $T\,/\,T_{\rm c} = 100$. This result is more in line with the common intuition that dynamically cold triples have a violent and short life, while virial triples are relatively calm and gradually build up their chaos in the long term.

As a further illustration of the influence of angular momentum, we provide a detailed comparison between low ($L = 0.02$) and high ($L = 0.19$) angular momentum triples in Fig. 8. In the lifetime histogram (top panel), we observe that a higher angular momentum indeed results in a larger fraction of long-lived triples. The difference in the lifetime distributions has two contributions. The first is that low-L triples have an initial phase of collapse since they start out in a sub-virial state, as opposed to the high-L virialised triples. This collapse causes more triples to dissolve in the first few crossing times. After that however, we observe that the two histograms also have a different slope. This indicates that bodies in a low-L system have a larger probability per crossing time to escape. In the main scatter plot, we also plot the corresponding fits to the upper ridge line in the data (from Figs 5–7). Since the slope in this plot corresponds directly to the Lyapunov exponent ($\lambda \propto \log A\,/\,T$), we notice that λ has a dependence on L, and since the slope in each curve flattens towards larger lifetimes, λ also depends on T. We have thus confirmed the general case in equation (19), where $\lambda = \lambda\,(L, T)$. The combination of longer lifetimes and larger Lyapunov exponents causes higher angular momentum triples to achieve increasingly larger amplification factors (see histogram in the right panel of Fig. 8).

We finish this subsection by deriving a relation between lifetime and Lyapunov time. Using equation (20), we can write

$$\log A = 10^{\beta}\left(\frac{T}{T_{\rm c}}\right)^{\alpha}. \tag{21}$$

Dividing both sides by $T\,/\,T_{\rm c}$ we obtain

$$\lambda T_{\rm c} = 10^{\beta}\left(\frac{T}{T_{\rm c}}\right)^{\alpha-1}, \tag{22}$$

or in terms of Lyapunov time:

$$\frac{T_\lambda}{T_{\rm c}} = 10^{-\beta}\left(\frac{T}{T_{\rm c}}\right)^{1-\alpha}. \tag{23}$$

Rewriting for T gives:

$$\frac{T}{T_{\rm c}} = 10^{\frac{\beta}{1-\alpha}}\left(\frac{T_\lambda}{T_{\rm c}}\right)^{\frac{1}{1-\alpha}}. \tag{24}$$

This expression describes a power-law relation between lifetime and Lyapunov time, corresponding to the maximum growth rate. The L-dependent power-law index of T_λ ranges from 3 to 8, which is much steeper than estimates from previous studies (e.g. Mikkola & Tanikawa 2007; Urminsky & Heggie 2009), although they focused on the median growth rate rather than the maximum rate. From equation (24) it may seem that triples with a shorter Lyapunov time-scale have shorter lifetimes. However, this statement assumes T_λ is a constant, such that if it were possible to measure a triple's instantaneous Lyapunov time-scale, one could predict its lifetime. However, this becomes problematic due to the large time variations in the rate of divergence, as we will discuss next.

3.3 Rate of divergence as a function of time.

In order to reach a deeper understanding of the physical origin of the empirical relations measured so far, it becomes necessary to closely correlate the instantaneous Lyapunov exponents to the orbital configurations. How do the triple components drive the growth of perturbations, and in general, how does that depend on angular momentum, mass ratio etc.? Although these are challenging but important questions requiring follow up studies, here we perform an analysis in the style of Dejonghe & Hut (1986). They define the metric

$$\mathrm{d}s^2 = \sum_{i=1}^{3}\sum_{j>i}\left(x_j - x_i\right)^2 + \left(y_j - y_i\right)^2 + \left(z_j - z_i\right)^2, \tag{25}$$

which is the sum of the squared distances between every pair of bodies. This metric is only small if all three bodies are close together, and during such moments amplifications are expected to be strong. On the other hand, if the metric attains very large values, then this corresponds to an excursion of one of the bodies from the bound pair. During such excursions the amplification is expected to be small. From our ensembles of simulations, we gather solutions with a fixed lifetime of 100 ± 2 crossing times. Then, for each ensemble of L we

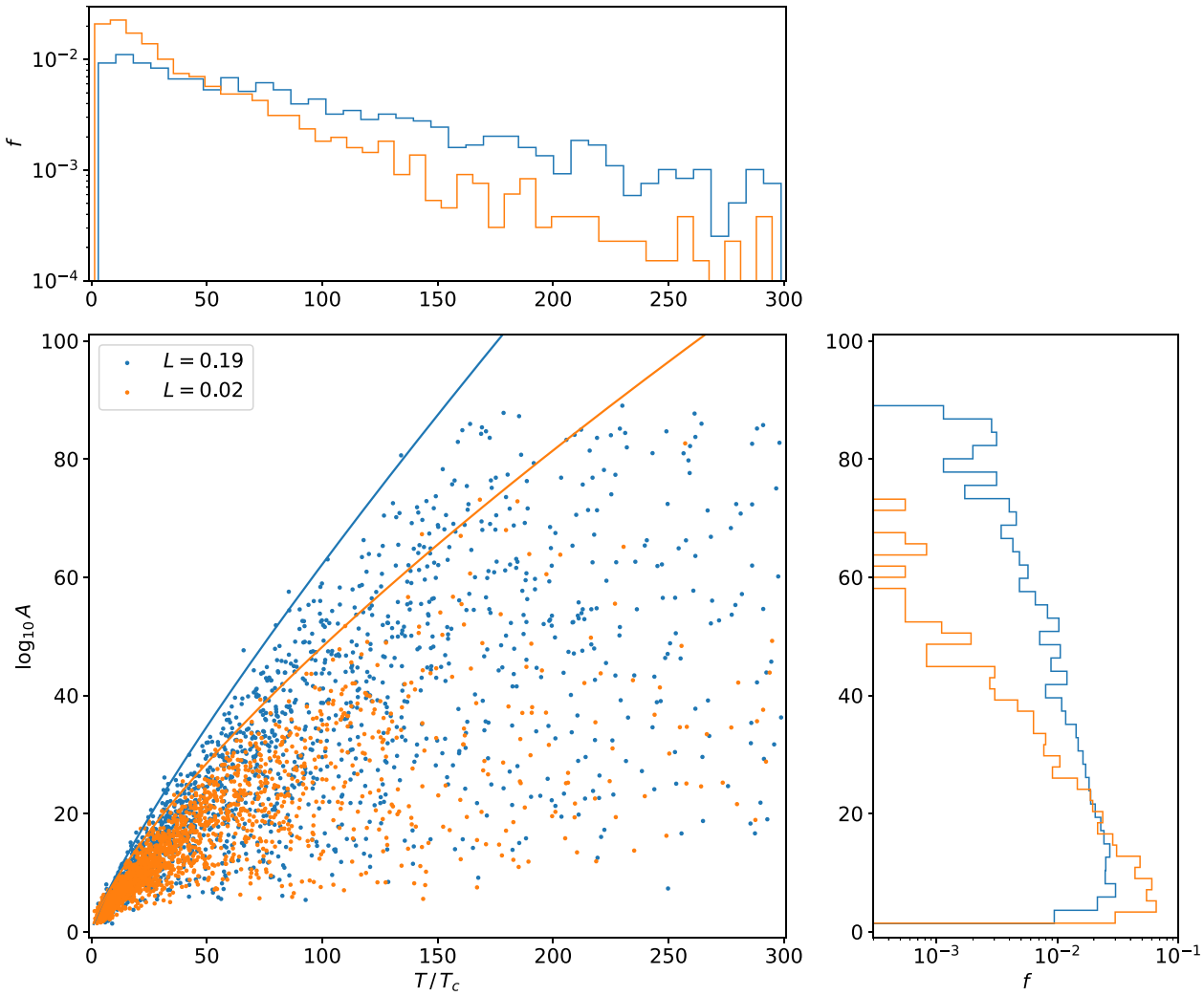

Figure 8. Relating the two main observables of the reversibility test: amplification factor, A, and lifetime, T. We compare the two most different ensembles given by $L = 0.02$ (orange/light) and $L = 0.19$ (blue/dark). We observe a bias both in the lifetime distribution (top histogram), and in the maximum achievable value of A given a certain value of T (scatter plot). The combination of longer lifetimes and larger growth rates leads to a larger fraction of high amplification factors (right histogram), and thus also a higher fraction of irreversible solutions (see Fig. 2).

select the solutions with the maximum and minimum amplification factor, i.e. the most and least chaotic solutions. We will make a comparison of these solutions between the most and least chaotic ensemble, $L = 0.19$ versus $L = 0.02$, and also between the low angular momentum ensembles, $L = 0$ versus $L = 0.02$. In Fig. 9, we compare the various solutions, and correlate the time evolution of the amplification factor with the metric defined above.

The metric shows an oscillatory behaviour indicating that the size of the triple itself oscillates. For the least chaotic solutions (those with the minimum values of A), we indeed observe that the metric attains large values (over a 100) and over an extended period (over 40 crossing times). The least chaotic solutions clearly correspond to very long excursions, during which the growth is linear. When the metric reaches a minimum value however, we observe a corresponding jump in A. This behaviour is consistent with punctuated chaos in which the rate of divergence is linear over extended times, but punctuated by big brief jumps due to strong events in the system, such as close encounters. According to this theory a higher frequency of events results in a more rapid amplification. The most chaotic solutions with the maximum values of A indeed correspond to a much higher oscillation frequency of the metric.

Sustained exponential growth is thus achieved if long excursions are absent, i.e. there is a prolonged democratic resonant interaction among the bodies. Comparing the most rapidly growing solutions for the three different values of L, we find that the number of events (i.e. minima of the metric) is not proportional to the rate of growth. For the most chaotic solution with $L = 0.19$ we count 50 oscillations, while for the least chaotic case $L = 0.02$ we count a similar 48 oscillations. For $L = 0$ we only count 28 oscillations, while still achieving a larger value of A than $L = 0.02$. Hence, we find that even during democratic resonant phases the growth is variable, indicating that other metrics also play a role. For example, considering the maximum $L = 0.02$ solution, we observe a rapid exponential growth between $40 \leq T/T_c \leq 50$, and a rather slow growth during $80 \leq T/T_c \leq 90$, even though both correspond to phases of high frequency of the metric with the same value of L.

The driver of chaos is therefore not (solely) close encounters in radial orbits, but rather the prolonged and non-linear interaction among all three bodies in a democratic configuration. Based on

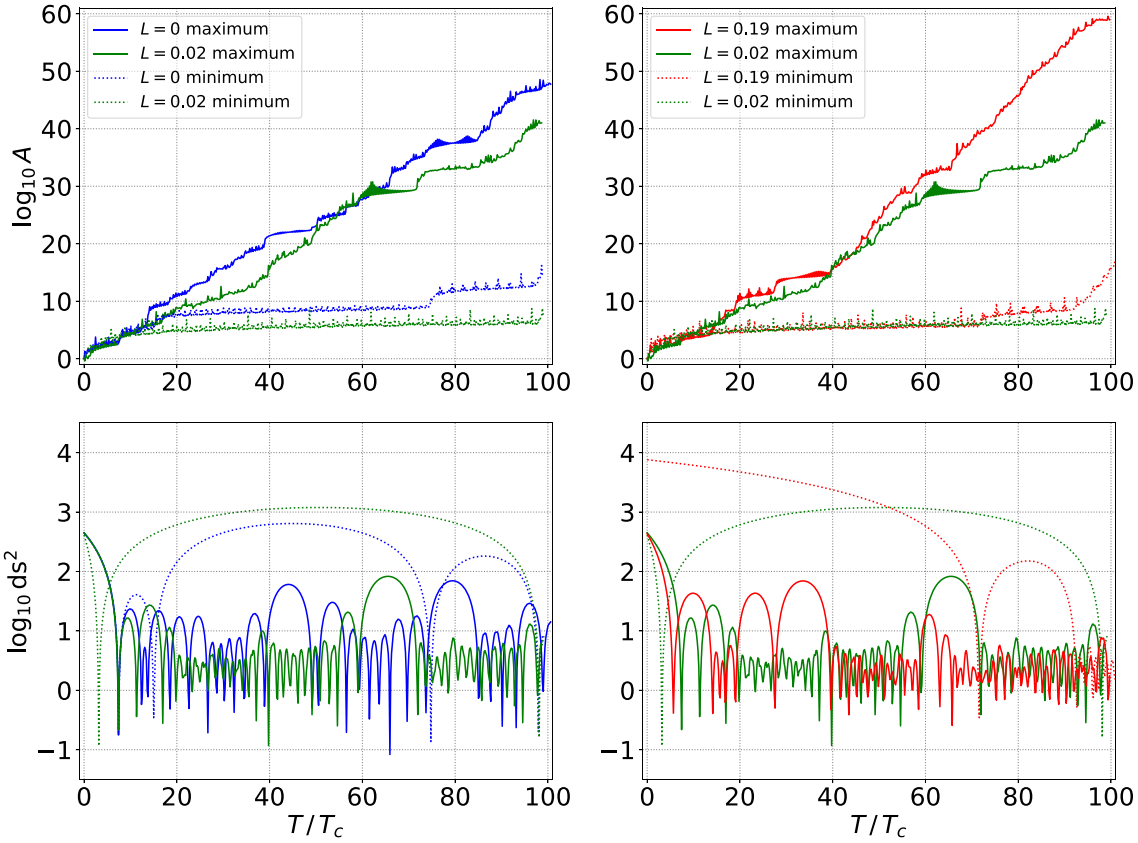

Figure 9. For triple systems with a lifetime of about 100 crossing times, we gather the solutions with the largest and smallest amplification factor. We plot the time evolution of the amplification factor (top panels), and of the metric ds^2 (bottom panels), which is the sum of the squared distances between all pairs. We compare the low angular momentum ensembles $L = 0$ and $L = 0.02$ (left column), and the most and least chaotic ensembles $L = 0.19$ and $L = 0.02$ (right column). Rapid growth is driven by democratic resonant interactions (high frequency oscillations in ds^2), while slow growth corresponds to long excursions of a single body from the bound pair.

our numerical results, we speculate that high angular momentum triples tend to have a longer cumulative resonant interaction time and/or shorter excursion phases of a single body, thereby effectively reducing the phases of slow growth. However, even during democratic three-body interaction phases the rate of divergence depends on other factors besides the metric ds^2, including L. This motivates a closer inspection of the dependence of the instantaneous Lyapunov exponent on the specifics of the orbital configuration in follow up studies.

4 DISCUSSION AND CONCLUSIONS

4.1 Angular momentum dependence

We revisit the astrophysical application of Paper 1, which considered three supermassive black holes with a mutual separation of order one parsec. In the zero angular momentum limit, we confirm their result that about 5 per cent of triples are irreversible up to the Planck length (see Table 1). This result is robust with respect to the type of initial condition (Plummer or Agekyan–Anosova map), as the most chaotic triples tend to forget their specific initial condition, and their ultimate fate is determined by global conserved quantities, i.e. angular momentum and energy.

Depending on the astrophysical context, triples with zero angular momentum might only represent a very small fraction of the population. Triple black holes in galactic centres, which form after repeated galaxy mergers, are expected to evolve to a hierarchical state at the edge of stability due to dynamical friction (e.g. Hoffman & Loeb 2007). Such weakly hierarchical triples fall within the highest angular momentum ensembles of our study. Hitherto, one might naively have expected that triples with a higher angular momentum might be less chaotic. This intuition mainly stems from the idea that chaos is driven by close encounters, which are more likely to occur in low angular momentum systems with radial orbits. Hence, it was expected that the 5 per cent of fundamentally unpredictable triples would be (greatly) reduced when considering a more general and realistic population of triples with varying, non-zero angular momenta. However, our results demonstrate the contrary; fundamentally unpredictable triples exist over a wide range of angular momenta, and the fraction of fundamentally unpredictable triples is even enhanced up to about 30 per cent of the population (for the initially virialised case).

We speculate that hierarchical triple systems near the edge of stability (e.g. Toonen et al. 2022), which can dynamically break up, also include a fraction of fundamentally unpredictable systems, similar to our highest angular momentum case. Increasing the angular momentum beyond the range studied here, will increase the hierarchy of the triple, thereby diminishing the effect of the tertiary on the inner binary. Although this increases the lifetime of the triple, it also increases the Lyapunov time-scale, with the net effect that Planck length perturbations will not be able to grow to the size of the triple any longer within any reasonable time-scale of interest. A natural extension of our study would be to probe this high angular momentum

Table 2. Fraction of fundamentally unpredictable triples for various astrophysical scales. For each system we give the characteristic mass and length scale, as well as the corresponding value of the dynamical crossing time. The minimum amplification factor required for a Planck length fluctuation to reach the size of the triple ($A_{\rm min}$) is also given. The fractions of irreversible systems are given by: p_h, for the intrinsic Planck length fluctuations (see Fig. 10), and $p_{\rm star}$, for the tidal perturbation from a star at a distance of 1 kpc (see Fig. 11). Each fraction is given as a range, where the lower limit is obtained from the $L = 0.02$ ensemble, and the upper limit from the virial $L = 0.19$ ensemble. We find that compact triples are more susceptible to Planck length perturbations, while tidal perturbations become increasingly important for larger triples. On the scale of dust grains, we find that both sources of perturbations become similar in magnitude.

Triple System	Mass scale (kg)	Length scale (m)	Crossing time (yr)	$\log_{10} A_{\rm min}$	$p_{\rm h}$(per cent)	$p_{\rm star}$(per cent)
Supermassive black holes	2.0×10^{36}	3.1×10^{16}	4.2×10^{4}	51.3	[0.031, 0.30]	[0.49, 0.77]
Stars	2.0×10^{30}	7.0×10^{12}	1.4×10^{2}	47.6	[0.040, 0.33]	[0.33, 0.68]
Jupiters	2.0×10^{27}	1.5×10^{11}	1.4×10^{1}	46.0	[0.046, 0.34]	[0.29, 0.64]
Moons	1.0×10^{21}	1.0×10^{8}	3.5×10^{-1}	42.8	[0.058, 0.37]	[0.22, 0.59]
Asteroids	1.0×10^{19}	7.7×10^{7}	2.3	42.7	[0.059, 0.37]	[0.25, 0.62]
Pebbles	1.0	3.3	6.6×10^{-2}	35.3	[0.10, 0.45]	[0.20, 0.57]
Dust grains	1.0×10^{-4}	1.0×10^{-3}	3.5×10^{-5}	31.8	[0.14, 0.49]	[0.12, 0.48]

region, and to determine for which value of the angular momentum the fraction of unpredictable triples peaks, and to measure at what rate this fraction subsequently decreases as the angular momentum is increased further. Since these triples would start out in a (stable) hierarchical configuration, contrary to the non-hierarchical systems studied here, it would be of interest to also study their Lyapunov times and amplification factors, and to link their behaviours to the underlying driver of chaos in terms of close encounter rates and resonances (e.g. Mardling & Aarseth 1999; Mardling 2008).

Another caveat for the existence of fundamentally unpredictable supermassive black hole triples is the effect of gravitational wave damping. For black hole masses above the transition mass scale of $\sim 10^7$ solar masses (e.g. Boekholt et al. 2021), the dynamics is merger-dominated, implying that a gravitational wave merger occurs (e.g. Hoffman & Loeb 2007), shortening the lifetime of the triple. Gravitational wave dissipation also quenches the exponential growth of perturbations if the damping time-scale becomes shorter than the Lyapunov time-scale. For black hole masses smaller than the transition mass, relativity acts as a perturbation to the system, such that a small change in the mass can lead to wildly different lifetimes of the triple interaction (Boekholt et al. 2021). If weakly hierarchical triples with masses of order 10^7 solar masses represent a fraction of realistic triple black holes in galaxies, then we estimate from our results that 20–30 per cent of them are fundamentally unpredictable due to Planck length fluctuations.

4.2 Dependence on astrophysical scale

It is also of interest to discuss how the fraction of fundamentally unpredictable triples depends on astrophysical scale. Although our purely Newtonian dynamical systems can be scaled up and down, here we will assume that there are physical constraints set by the Planck length and the Hubble time. We consider scatter plots similar to that of Fig. 8, where the Hubble time introduces a maximum cut-off in $T\,/\,T_{\rm c}$, and where the Planck length introduces a minimal value of A above which systems are considered to be fundamentally unpredictable. For various physical scalings of the triple system we can then count the fraction of triples in the fundamentally unpredictable region of the diagram.

The critical 'Hubble scale' can be defined which gives the limit where a triple is just able to magnify a Planck length perturbation to its own size on a time-scale of a Hubble time. The minimum amplification required is defined as the size of the triple, R, divided by the Planck length, h. This amplification is to be reached within a Hubble time, $T_{\rm H}$. Using the relation between A amd T from equation (20), we can write

$$\log_{10} A_{\rm min} \equiv \log_{10} \frac{R}{h} = 10^{\beta} \left(\frac{T_{\rm H}}{T_{\rm c}} \right)^{\alpha}, \tag{26}$$

with α and β the fitting parameters given in Table 1. The crossing time of a virialised N-body system can be expressed as (see Section 2.1)

$$T_{\rm c} = \sqrt{\frac{8R^3}{GM}}. \tag{27}$$

Replacing this expression into equation (26) and rewriting for M, we obtain

$$M_{\rm H} \equiv 8 \times 10^{-\frac{2\beta}{\alpha}} G^{-1} T_{\rm H}^{-2} R^3 \left(\log_{10} \frac{R}{h} \right)^{\frac{2}{\alpha}}. \tag{28}$$

Hence, given a triple of physical size R, if its mass $M > M_{\rm H}$, then the triple's crossing time is sufficiently small for it to be able to magnify a Planck length perturbation up to its own size.

In Table 2, we list various types of bodies which could be part of a triple system; from large scale supermassive black holes down to asteroids, pebbles and dust grains. For each type we give the characteristic mass and length scale, as well as their crossing time. The minimum amplification factor required to magnify a Planck length perturbation to the size of the triple itself is also given, ranging from 10^{32}–10^{51}. In Table 2 we also give the percentage of unpredictable triples due to quantum uncertainties, p_h, as a range, where the lower limit is calculated from the least chaotic ensemble ($L = 0.02$) and the maximum from the most chaotic ensemble ($L = 0.19$). We visualise the most chaotic case in Fig. 10, where we also overplot the locations of the various astrophysical bodies. The general trend is that the fraction of fundamentally unpredictable triples increases for more compact triples. Smaller systems require a smaller amplification of the Planck length in order to become unpredictable.

Hence, by increasing the angular momentum of supermassive black hole triples, the fraction of unpredictable systems is enhanced from 5 per cent to 30 per cent, and by decreasing the scale of the triple down to triple dust grains, the percentage is further enhanced to about 50 per cent. Fundamentally unpredictable triples are general, occurring over a large range of astrophysical scales owing to the exponential nature of chaos.

4.3 Small perturbations from the rest of the Universe

In Paper 1 and in this current study, we focused on perturbations due to intrinsic quantum uncertainties. We assumed that these form

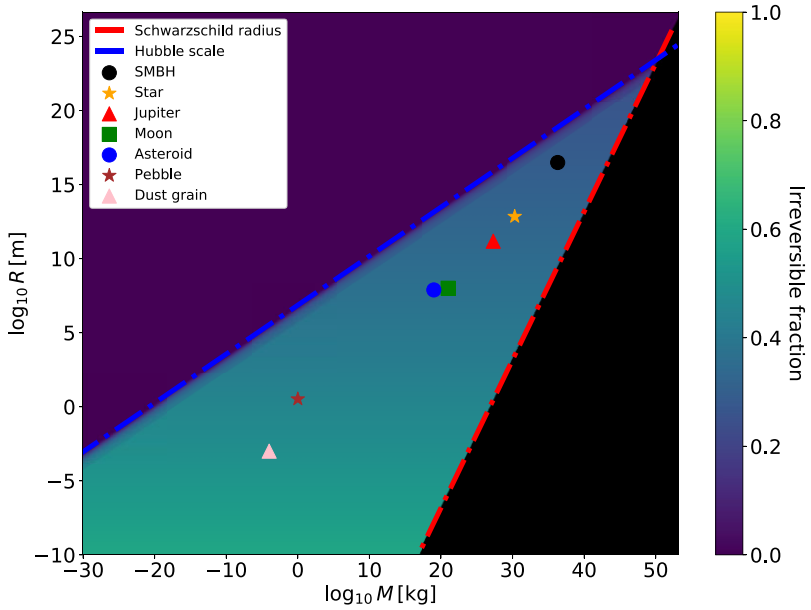

Figure 10. Fraction of fundamentally unpredictable triples as a function of astrophysical scale. The mass scale ranges from the electron mass to the estimated total baryonic mass in the Universe, and the length scale ranges from the size of an atom to the size of the observable Universe. Two characteristic lines divide the region in (mostly) three large subregions. The bottom right region is excluded due to densities exceeding those of black holes (Schwarzschild radius determines the lower edge of the central area marked by a dash-dotted line). The upper left triangular region corresponds to fundamentally predictable triples as they are unable to magnify Planck length perturbations to their own system size within a Hubble time. The analytical expression for the 'Hubble scale' (upper dash-dotted line) is given in equation (28). In the middle region, the trend is that the fraction increases towards smaller length scales; a smaller amplification of the Planck length is required to reach the size of the triple. The locations of various astrophysical bodies are overplotted, e.g. for triple supermassive black holes (SMBH) 30 per cent are irreversible, and this increases to 37 per cent for triple asteroids and 49 per cent for dust grains. Here, we assumed the triples are virial ($L = 0.19$), but in Table 2 we also provide values for the least chaotic chase ($L = 0.02$).

the smallest physical perturbations in nature, and demonstrated that they still play a role in the predictability of triple systems (and therefore in larger-N systems too). However, there are other sources of perturbations in the Universe, which can be much larger in magnitude. For example, we can compare the evolution of an isolated triple system to one with a fourth-body at some large distance from the triple. This external body will induce a tidal effect onto the triple, causing each of the triple components to experience a slightly different tidal acceleration. In the centre of mass frame of the triple this will manifest as slight perturbations in the orbits of the bodies (compared to the isolated triple case). The magnitude of these tidal seed perturbations depends on the distance of the fourth body, and we ask at what distance does the tidal perturbation become of the same order as the Planck length? The tidal acceleration is estimated as

$$\delta a \sim \frac{G m_{\rm t} R}{(\gamma R)^3} = \frac{G m_{\rm t}}{\gamma^3 R^2}, \tag{29}$$

with G the gravitational constant, $m_{\rm t}$ the mass of the tidal perturber, and R the size of the triple. The factor γ gives the distance of the fourth-body in units of R. The accelerations within the triple are of order $a \sim \frac{GM}{R^2}$, with M the mass of the triple. We can estimate the seed perturbation in the orbit according to $\frac{\delta r}{R} \sim \frac{\delta a}{a}$, allowing us to write

$$\delta r \sim R\frac{\delta a}{a} = \frac{R}{\gamma^3}\frac{m_{\rm t}}{M}. \tag{30}$$

Setting δr equal to the Planck length, h, we obtain the characteristic separation of

$$\gamma_h = \left(\frac{R}{h}\frac{m_{\rm t}}{M}\right)^{\frac{1}{3}}. \tag{31}$$

We compare this separation to the size of the observable Universe, $R_{\rm U} = \gamma_{\rm U} R$, so that we finally obtain

$$\frac{\gamma_h}{\gamma_{\rm U}} = \left(\frac{R^4}{h R_{\rm U}^3}\frac{m_{\rm t}}{M}\right)^{\frac{1}{3}}. \tag{32}$$

Now we will assume that the fourth body is of the same type as the triple components, i.e. $m_{\rm t} \sim M$. Furthermore, by setting $\gamma_h = \gamma_{\rm U}$, we obtain the following characteristic length scale:

$$R_h \equiv h^{\frac{1}{4}} R_{\rm U}^{\frac{3}{4}} \approx 1\,\text{au}. \tag{33}$$

Triple systems larger than this surprisingly small length scale, will be susceptible to tidal perturbations of order the Planck length due to bodies beyond the cosmological horizon. For more compact triples, such distant tidal perturbations will be negligible compared to the intrinsic quantum uncertainty.

In reality, there will be many tidal perturbers much closer to home. For example, for our standard test case supermassive black hole triple, there are billions of perturbing stars in the host galaxy. Using equation (30), with $M = 10^6\,{\rm M}_\odot$, $R = 1\,{\rm pc}$, $m_{\rm t} = 1\,{\rm M}_\odot$, and $\gamma = 10^3$, we estimate a seed perturbation of $\delta r = 30\,{\rm m}$ in the orbits of the black holes. Magnifying this to the size of the triple requires an amplification factor of only $R/\delta r \sim 10^{15}$. Similar to the previous subsection, we can count the fraction of triple systems that reach an amplification factor larger than 10^{15} within a Hubble time, which

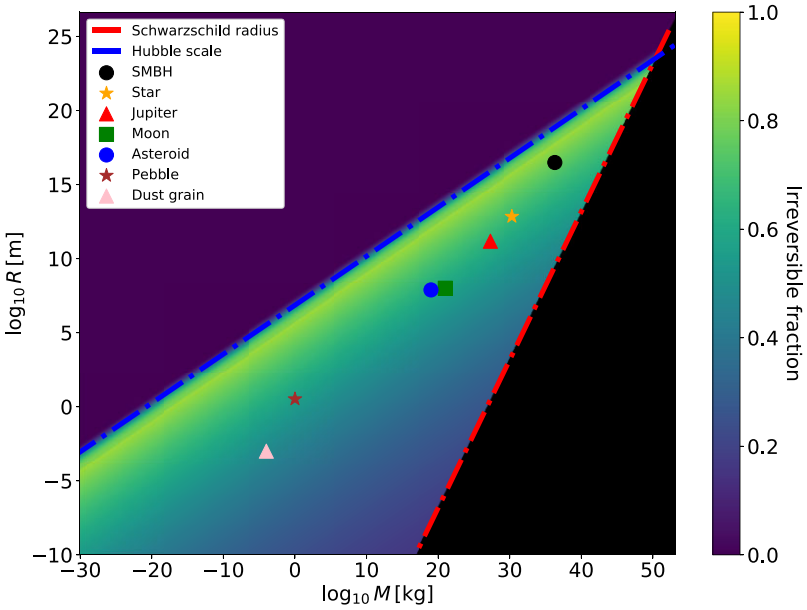

Figure 11. Similar plot as Fig. 10, but for tidal perturbations on the triple system due to a Solar mass star at a distance of 1 kpc. As this example shows, small tidal perturbations from other bodies in the Universe play an important role in the predictability of triple systems. Especially for the relatively loosely bound triples with the largest crossing times, i.e. near to the 'Hubble scale'. Generally, tidal perturbations tend to dominate over intrinsic quantum fluctuations. As a consequence, the fraction of irreversible triples increases; up to 77 per cent for triple supermassive black holes (see Table 2).

ranges from 49–77 per cent depending on L. For smaller scale triples, the fraction of unpredictable triples due to tidal perturbations tends to decrease, e.g. down to 25–62 per cent for asteroids and 12–48 per cent for dust grains (see Table 2). In Fig. 11, we visualise these percentages and we observe that tidal perturbations mostly affect the loosely bound triples, i.e. those with the largest crossing times near the Hubble scale. Generally, external tidal perturbations from other bodies in the Universe tend to dominate over intrinsic quantum uncertainties.

4.4 Future work

The contradiction between the naive expectation that lower-L systems would be maximally chaotic, and our new numerical results motivates further investigation into the origin of chaos in triple systems, as well as larger N-body systems (e.g. Portegies Zwart et al. 2022; Portegies Zwart & Boekholt 2023). Although it is well known that higher angular momentum triples tend to live longer on average, here we find that they can also have larger maximum Lyapunov exponents (shorter Lyapunov times). The driver of chaos is therefore not (solely) close encounters in radial orbits, but rather the prolonged and non-linear interaction among all three bodies in a democratic configuration. However, we find that even during such democratic resonances the rate of divergence can vary. Based on our numerical results, we speculate that high angular momentum triples might statistically have a longer cumulative resonant interaction time and/or shorter excursion phases of a single body. This requires a closer inspection of the dependence of the instantaneous Lyapunov exponent on the specifics of the orbital configuration.

ACKNOWLEDGEMENTS

We kindly thank the referee for suggesting clarifications and interpretations, which improved the presentation of our results. We acknowledge the valuable feedback received on this project during the Chaotic Rendez-Vous meeting in Edinburgh in 2023 organised by Anna Lisa Varri. The calculations were performed using the LGMII (Nederlandse Organisatie voor Wetenschappelijk Onderzoek, NWO, grant #621.016.701). Part of this publication is funded by the Nederlandse Onderzoekschool Voor Astronomie (NOVA). TB's research was supported by an appointment to the NASA Postdoctoral Program at the NASA Ames Research Center, administered by Oak Ridge Associated Universities under contract with NASA.

DATA AVAILABILITY

The data underlying this article will be shared on reasonable request to the corresponding author.

REFERENCES

Agekyan T. A., Anosova Z. P., 1967, Astron. Zh., 44, 1261
Agekyan T. A., Anosova Z. P., 1968, Astron. Zh., 11, 1006
Boekholt T., Portegies Zwart S., 2015, Comput. Astrophys. Cosmol., 2, 2
Boekholt T. C. N., Pelupessy F. I., Heggie D. C., Portegies Zwart S. F., 2016, MNRAS, 461, 3576
Boekholt T. C. N., Portegies Zwart S. F., Valtonen M., 2020, MNRAS, 493, 3932 (Paper 1)
Boekholt T. C. N., Moerman A., Portegies Zwart S. F., 2021, Phys. Rev. D, 104, 083020
Boekholt T. C. N., Portegies Zwart S. F., Heggie D. C., 2023a, Int. J. Mod. Phys. D, 32, 2342003
Boekholt T. C. N., Rowan C., Kocsis B., 2023b, MNRAS, 518, 5653
Correia A. C. M., 2018, Icarus, 305, 250
Dejonghe H., Hut P., 1986, in Hut P., McMillan S. L. W., eds, Lecture Notes in Physics, Vol. 267, The Use of Supercomputers in Stellar Dynamics. Springer-Verlag, Berlin, p. 212
Goodman J., Heggie D. C., Hut P., 1993, ApJ, 415, 715
Heggie D. C., Mathieu R. D., 1986, in Hut P., McMillan S. L. W., eds, Lecture Notes in Physics, Vol. 267, The Use of Supercomputers in Stellar Dynamics. Springer-Verlag, Berlin, p. 233
Hoffman L., Loeb A., 2007, MNRAS, 377, 957

Kepler J., 1609, Astronomia nova..., seu physica coelestis, tradita commentariis de motibus stellae martis. E. Vögelin, Heidelberg
Kollatschny W., Weilbacher P. M., Ochmann M. W., Chelouche D., Monreal-Ibero A., Bacon R., Contini T., 2020, A&A, 633, A79
Manwadkar V., Trani A. A., Leigh N. W. C., 2020, MNRAS, 497, 3694
Mardling R. A., 2008, in Aarseth S. J., Tout C. A., Mardling R. A.eds, The Cambridge N-Body Lectures. Springer, Berlin, 760, 59
Mardling R., Aarseth S., 1999, in Steves B. A., Roy A. E.eds, NATO Advanced Study Institute (ASI) Series C Vol. 522, The Dynamics of Small Bodies in the Solar System, A Major Key to Solar System Studies. Kluwer Academic Publishers, p.385
McMillan S. L. W., Hut P., 1996, ApJ, 467, 348
Mikkola S., Tanikawa K., 2007, MNRAS, 379, L21
Miller R. H., 1964, ApJ, 140, 250
Newton I., 1687, in Halley E., Pepys S. (eds), Philosophiae naturalis principia mathematica. London
Orlov V. V., Rubinov A. V., Shevchenko I. I., 2010, MNRAS, 408, 1623
Plummer H. C., 1911, MNRAS, 71, 460
Poincaré H., 1891, Bulletin Astronomique, Serie I, 8, 12
Poincaré H., 1892, Les methodes nouvelles de la mecanique celeste. Gauthier-Villars et Fils (Paris), Paris
Portegies Zwart S., Boekholt T., 2014, ApJ, 785, L3
Portegies Zwart S. F., Boekholt T. C. N., 2018, Commun. Nonlinear Sci. Numer. Simul., 61, 160
Portegies Zwart S., Boekholt T., 2023, AIP Conf. Proc. Vol. 2832, The paradox of infinitesimal granularity: Chaos and the reversibility of time in Newton's theory of gravity. Am. Inst. Phys., New York, p. 050003
Portegies Zwart S. F., McMillan S. L. W., 2000, ApJ, 528, L17
Portegies Zwart S. F., Boekholt T. C. N., Por E. H., Hamers A. S., McMillan S. L. W., 2022, A&A, 659, A86
Portegies Zwart S. F., Boekholt T. C. N., Heggie D. C., 2023, MNRAS, 526, 5791
Samsing J., MacLeod M., Ramirez-Ruiz E., 2014, ApJ, 784, 71
Stone N. C., Leigh N. W. C., 2019, Nature, 576, 406
Toonen S., Boekholt T. C. N., Portegies Zwart S., 2022, A&A, 661, A61
Touma J., Wisdom J., 1998, AJ, 115, 1653
Trani A. A., Leigh N. W. C., Boekholt T. C. N., Portegies Zwart S., 2024, A&A, 689, A24
Urminsky D. J., Heggie D. C., 2009, MNRAS, 392, 1051
Väisänen P. et al., 2008, MNRAS, 384, 886

This paper has been typeset from a TEX/LATEX file prepared by the author.